Journal of Power Sources 184 (2008) 238–244

Contents lists available at ScienceDirect

Journal of Power Sources

journal homepage: www.elsevier.com/locate/jpowsour

Effect of pre-oxidation and environmental aging on the seal strength of a novel high-temperature solid oxide fuel cell (SOFC) sealing glass with metallic interconnect

Yeong-Shyung Chou*, Jeffry W. Stevenson, Prabhakar Singh

K2-44, Materials Department, Pacific Northwest National Laboratory, P.O. Box 999, Richland, WA 99354, United States

ARTICLE INFO

Article history:
Received 19 May 2008
Received in revised form 2 June 2008
Accepted 6 June 2008
Available online 20 June 2008

Keywords:
Seal strength
Sealing glass
Interface
Crofer22APU
SOFC

ABSTRACT

A novel high-temperature alkaline-earth silicate sealing glass was developed for solid oxide fuel cell (SOFC) applications. The glass was used to join two ferritic stainless steel coupons for strength evaluation. The steel coupons were pre-oxidized at elevated temperatures to promote thick oxide layers to simulate long-term exposure conditions. In addition, seals to as-received metal coupons were also tested after aging in oxidizing or reducing environments to simulate the actual SOFC environment. Room temperature tensile testing showed strength degradation when using pre-oxidized coupons, and more extensive degradation after aging in air. Fracture surface and microstructural analysis confirmed that the cause of degradation was formation of $SrCrO_4$ at the outer sealing edges exposed to air.

© 2008 Elsevier B.V. All rights reserved.

1. Introduction

Solid oxide fuel cells (SOFCs) have received much attention in recent years due to anticipated depletion of fossil fuels, increasing electricity demand, and the need for greener technologies to fight against climate change. Unlike conventional combustion engines/turbines, SOFCs generate electricity by electrochemical at elevated temperatures reaction rather than combustion. As a result, higher energy efficiency and less pollutants are expected [1,2]. Potential markets of interest to industrial developers include stationary and transportational applications. Currently, there are two generic designs of SOFCs: tubular and planar [3–5]. The latter approach involves stacking of tens of repeating unit cells (anode/electrolyte/cathode) separated by metallic interconnect plates. Sealing technology is needed to prevent direct mixing of fuel with oxidizer for the SOFC stack to function properly. The sealing materials have to provide hermeticity or low leak rate, and must be electrically insulating, chemically compatible with mating materials, thermally stable, and durable in the harsh dual operating environment (oxidizing vs. wet reducing atmospheres). The seals must survive thermal cycling as well as long-term (e.g., ~40,000 h) operation at elevated temperatures (~700–850 °C).

In general, SOFC sealing approaches can be classified into three categories: glass and glass-ceramic seals [6–14], silver-based active brazes [15–18], and mica-based compressive seals [19–21]. Each one has its own advantages and disadvantages, as addressed in recent reviews [22,23]. Among these approaches, glass and glass-ceramics have been most extensively studied. Chou et al. studied a novel $SrO–CaO–Y_2O_3–SiO_2–B_2O_3$ glass system with focus on higher sealing temperatures (>950 °C) for better long-term thermal and chemical stability by varying the B_2O_3 content [6]. Results showed very stable microstructure and crystalline phases after 2000 h aging at 900 °C. Lahl et al. studied the crystallization kinetics of $AO-Al_2O_3–SiO_2–B_2O_3$ glasses (A = Ba, Ca and Mg) and the influence of nucleating agents (TiO_2, ZrO_2 and Cr_2O_3) on the activation energy for crystal growth [7]. They found that the activation energy for crystal growth was increased by most nucleating agents except ZrO_2, and the preparation method determined whether surface or bulk nucleation was the dominant mechanism. Sohn et al. investigated the thermal and chemical stability of the $BaO–Al_2O_3–La_2O_3–SiO_2–B_2O_3$ system. They found that the CTE increased with BaO content and a maximum CTE of $\sim 11 \times 10^{-6}\,°C^{-1}$ was obtained at BaO = 40% and $B_2O_3/SiO_2 = 0.7$. The thermal properties of the crystallized glasses were not reported [8]. Ley et al. studied the glass system of $SrO–Al_2O_3–La_2O_3–SiO_2–B_2O_3$. The coefficients of thermal expansion (CTE) of the as-prepared glasses were in the range of $8–13 \times 10^{-6}\,°C^{-1}$ [9]. Adding ceramic fibers into the seal-

* Corresponding author. Tel.: +1 509 3752527; fax: +1 5093752186.
E-mail address: yeong-shyung.chou@pnl.gov (Y.-S. Chou).

0378-7753/$ – see front matter © 2008 Elsevier B.V. All rights reserved.
doi:10.1016/j.jpowsour.2008.06.020

Table 1
Chemical composition range of Crofer22APU metal coupons used for seal strength tests

wt.%	Cr	Fe	C	Mn	Si	Cu	Al	S	P	Ti	La
Minimum	20.00	Balance		0.30						0.03	0.04
Maximum	24.00	Balance	0.03	0.80	0.50	0.50	0.50	0.02	0.05	0.20	0.20

Data from manufacturer (Thyssenkrupp VDM GmbH, Germany).

ing glass was demonstrated by Taniguchi et al. to improve the thermal cycle stability [10]. However, the seal was complex, consisting of three layers: a glass plate, a ceramic fiber layer, and a composite layer of glass and YSZ powders. As a result, high compressive applied stress (2 kgf cm^{-2}, ~29 psi) was needed. In addition to the CTE match, minimal interfacial reaction with adjacent components is also required for sealing glasses. As the operation temperature for SOFC has dropped from ~1000 °C to below ~800 °C, the use of metals as the interconnect plate has become possible. However, glass/metal interactions can degrade the mechanical properties of the seals. The behavior of various glass-ceramics with ferritic stainless steels under SOFC environments was investigated [11–14], and the results for as-sealed or short-term aged (<400 h) samples showed undesirable chromate formation [6,14], microstructure degradation, and electrical short circuiting [12]. None of these studies investigated the mechanical properties of the seal, which are important in advancing SOFC technologies since typical SOFC stack life expectancy is around 40,000 h with numerous thermal cycles during routine operation. Thus, a robust seal is a must for the stack to survive transient as well as residual stresses during thermal cycling. The objective of this study was to investigate the seal strength of a novel high-temperature sealing glass with a candidate steel interconnect material (Crofer22APU) and to identify the cause of failure. Effects of environmental aging and oxide layer thickness were also studied. Fracture surface and microstructure analyses were conducted and correlated with the strength testing results.

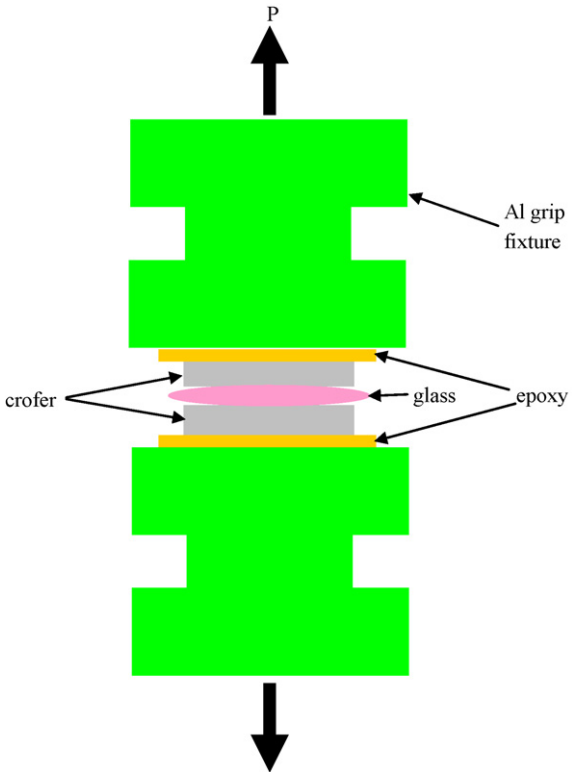

Fig. 1. A schematic drawing showing the tensile testing assembly with a sealed metal couple bonded to the Al grips with epoxy.

2. Experimental

2.1. Raw materials and sample preparation

The sealing glass used in this study is a high-temperature (SrO,CaO)–Y_2O_3–B_2O_3–SiO_2 glass (YSO75) which was prepared by melting of oxides and carbonates at 1500 °C in a Pt crucible. The details of glass fabrication and heat-treatment are given in Ref. [6]. The as-cast bulk glass was crushed and ground in a WC vibratory mill for two minutes and sieved through a #100 mesh sieve. Thermal properties of the as-cast glass and glass powder compacts sintered at 950 °C for 2 h followed by 800 °C for 4 h were measured with a dilatometer (Unitherm 1161, ANTER Corp., Pitts-

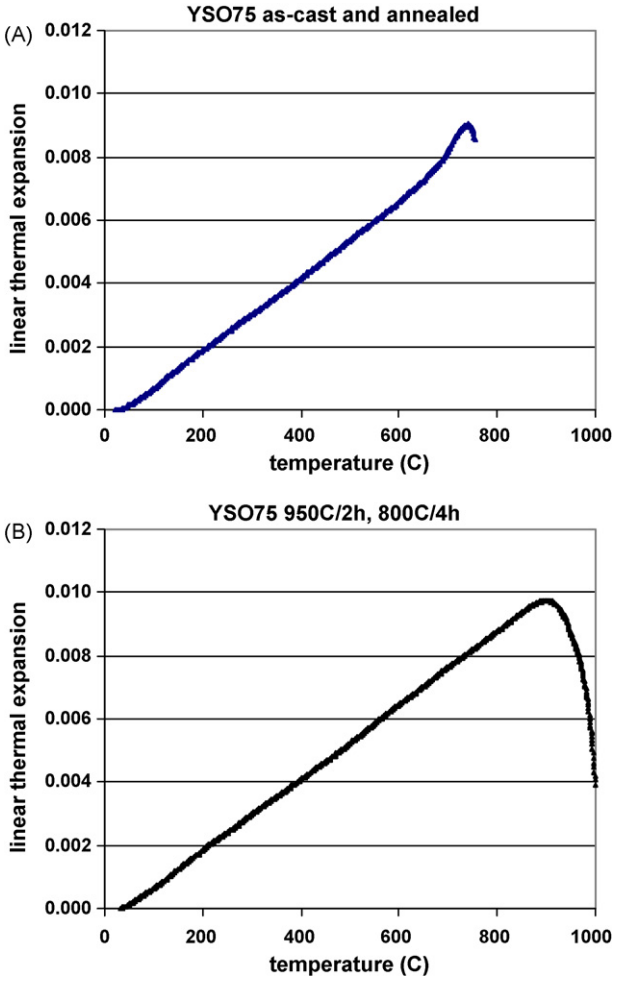

Fig. 2. Linear thermal expansion curves of glass YSO75: (A) as-cast and annealed bulk glass, and (B) glass powder compact after short-term crystallization in air at 950 °C/2 h and 800 °C/4 h.

Table 2
Thermal properties of the sealing glass

Condition	T_g (°C)	T_s (°C)	Average CTE ($\times 10^{-6}$/°C)
As-cast bulk glass	685	741	11.63
Short-term crystallized	N/A	914	11.87

Note: Average CTE of the as-cast glass was for temperature range from RT to T_g; average CTE of the short-term crystallized glass was from RT to T_s.

burgh, PA) using rectangular bars about 27 mm long. The glass powders were also mixed with an organic binder (V-006, Heraeous Electronic Materials, W. Conshohocken, PA) to form a paste for sealing. The Crofer22APU steel coupons used for sealing and strength tests 12.5 mm × 12.5 mm × 1 mm. The compositional range for Crofer 22APU, a special ferritic stainless steel developed for SOFC applications, is listed in Table 1. Test specimens were prepared by applying the glass paste to two metal coupons to form steel/glass paste/steel sandwiches. After drying, the specimens were slowly heated to 550 °C for 2 h to remove organic binders. They were then heated to 975 °C for 2 h followed to 800 °C for 4 h (short-term crystallization). To study the oxide layer thickness effects, metal coupons were pre-oxidized in air at 800, 1000 or 1200 °C for 2 h. To study effects of environmental aging, as-sealed specimens were either aged in air at 850 °C for 500 h or aged in a wet (~30% H_2O) dilute hydrogen (2.7% H_2/Ar) atmosphere at 850 °C for 250 h.

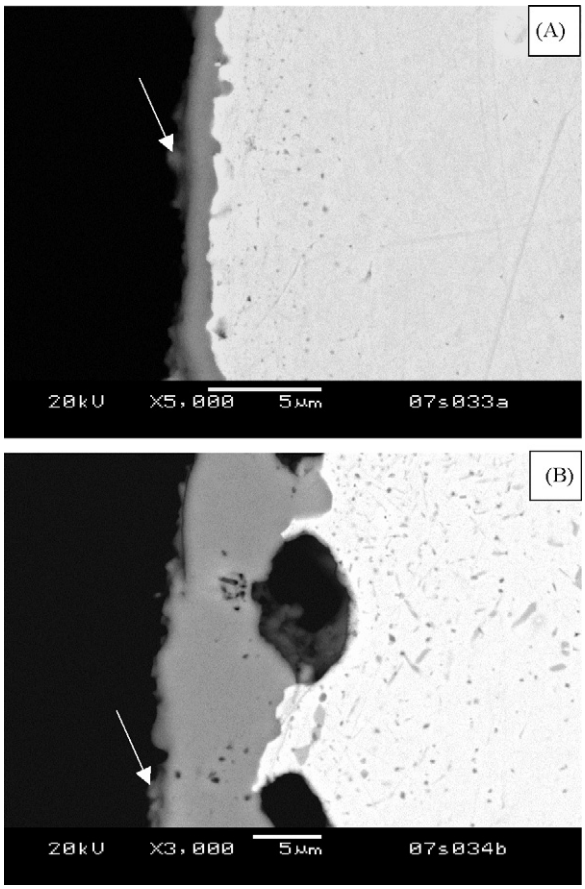

Fig. 3. SEM images showing the oxide scale (primarily Cr_2O_3) on pre-oxidized Crofer22APU metal coupons: (A) pre-oxidized at 1000 °C/2 h and (B) pre-oxidized at 1200 °C/2 h. Arrows in the figures show the top layer of $(Cr,Mn)_3O_4$ spinel.

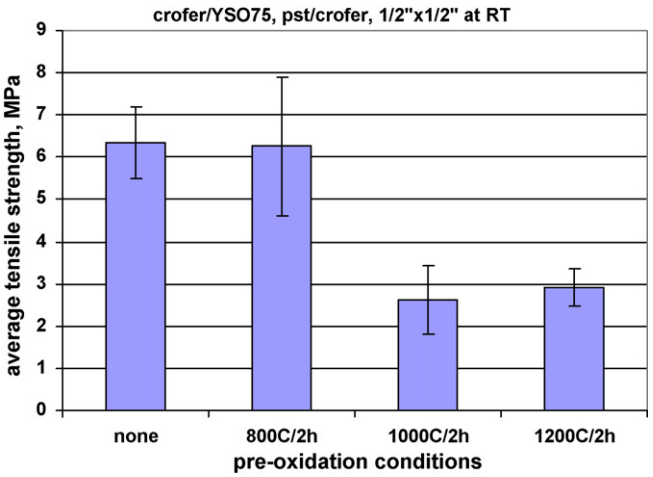

Fig. 4. Effect of pre-oxidation of the metal coupons on the room temperature seal strength.

2.2. Mechanical testing and microstructural characterization

For room temperature seal strength tests, the sealed metal coupons were glued to two aluminum test fixtures using fast-setting epoxy as shown in Fig. 1. The assembly was then tested in uniaxial tension using a mechanical tester (MTS Bionix 400, MTS Canton, MA) with a cross-head speed of 0.5 mm min^{-1} in ambient conditions. The fixture had a self-alignment joint to minimize bending or twisting during tensile testing. For each condition, about 6–7 samples were tested and the average strength was determined. After the test, fracture surfaces were examined with optical microscopy. Some of the samples were also epoxy mounted, sectioned, and polished for interfacial characterization using scanning electron microscopy (JOEL SEM model 5900LV).

3. Results and discussion

3.1. Thermal properties of high-temperature sealing glass

The sealing glass (YSO75) used in this study is a high-temperature sealing glass. While conventional sealing glasses for SOFC stacks operated at ~800 °C typically have a sealing temperature of ~825–850 °C, the sealing temperature of glass YSO75 is

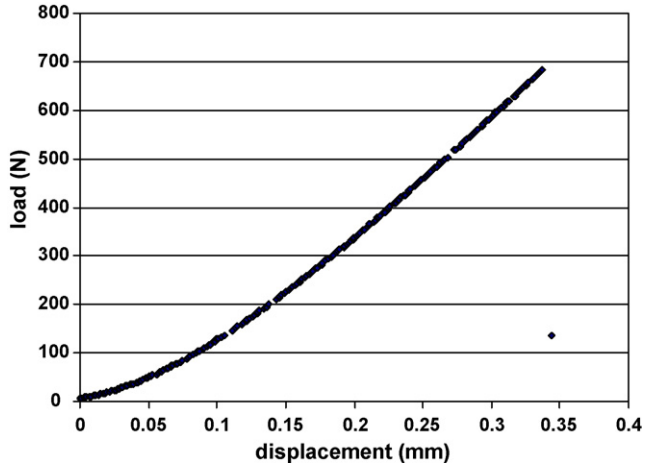

Fig. 5. Load and displacement curve of the room temperature seal strength test of as-sealed as-received Crofer22APU. The curve shows typical brittle failure.

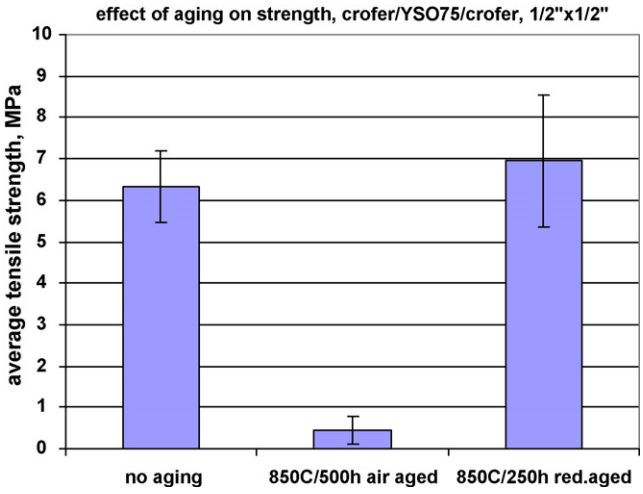

Fig. 6. Effect of environmental aging on the room temperature seal strength.

~950–1000 °C. Higher sealing temperatures allowed for compositional modifications which resulted in improved thermal and electrical properties of the glass, and are also expected to result in improved sintering and hence higher bonding strength and conductivity of the contact materials at the cathode/interconnect interface. Satisfactory contact bonding during long-term operation and thermal cycling is critical because poor contact results in high ohmic resistance and therefore poor electrochemical performance.

The linear thermal expansion of glass YSO75 is shown in Fig. 2A for the as-cast and annealed bulk glass, and in Fig. 2B for a short-term crystallized glass powder compact. Thermal properties (glass transition temperature (T_g), dilatometric softening point (T_s), and coefficient of thermal expansion) are listed in Table 2. The as-cast and annealed bulk glass showed a typical expansion curve for glass, with a distinct glass transition point (T_g = 685 °C) and dilatometric softening point (T_s = 741 °C). The short-term crystallized glass did not exhibit a normal glass transition point but did soften at 914 °C, suggesting the glass power compact had crystallized substantially but still contained residual glassy phase. It should be noted that glass YSO75 exhibits a CTE that is well matched with other SOFC stack components including Ni/YSZ anode-supported cells and ferritic stainless steel interconnect materials (~12.5×10^{-6} °C^{-1}).

3.2. Pre-oxidation of Crofer22APU

For SOFC stacks operating at temperatures ≤800 °C, metallic interconnects are favored over ceramic interconnects due to higher electrical and thermal conductivity and lower cost. Conductive chromia scale forming ferritic stainless steels are the leading candidates. Among these candidates, Crofer22APU has been studied extensively due to its excellent CTE match with Ni/YSZ anode-supported cells and good oxidation resistance. The bonding/wetting behavior of silicate glasses to metals is strongly dependent on the nature of the surface of the metal. Metallic surfaces often result in poor joining due to poor wetting, while an oxide layer on the metal surface tends to promote wetting which leads to improved chemical bonding. As the metallic interconnect is exposed to a dual environment of fuel and air at elevated temperatures during SOFC operation, oxidation of the metal is inevitable, with the thickness of the oxide scale on the surface increasing over time. Extensive oxidation can lead to cracking and/or spallation at the scale/metal interface leading to degradation of seal strength and integrity. Oxidation rates at seal/interconnect interfaces will be substantially reduced if the seal material is sufficiently dense to effectively prevent oxygen transport to the interconnect surface; protective interconnect coatings can also greatly assist in minimizing scale growth.

As the service life of planar SOFCs may be 40,000 h or more, it is critical to know the effect of scale thickness on seal strength. To simulate long-term operation, Crofer22APU coupons were pre-oxidized in air at various elevated temperatures to promote different thickness of chromia scales. Fig. 3 shows the cross-section view of samples pre-oxidized at 1000 °C/2 h and 1200 °C/2 h. The oxide thickness of 1000 °C/2 h pre-oxidized samples was about 1–2 μm, and 6–10 μm for 1200 °C/2 h oxidized ones. The growth of chromia scale frequently follows a classical parabolic law. Published chromia scale growth rate constants varied substantially. For example, Fontana et al reported a scale growth rate constant of 4.8×10^{-14} g^2 cm^{-4} s^{-1} for Crofer22APU (2 mm thick) at 800 °C [24]. Huczkowski et al., however, found the growth constants were dependent on sample thickness due to exhaustion of Cr reservoir and break-away phenomenon for thin samples, and a much higher rate constant of 1.0×10^{-12} g^2 cm^{-4} s^{-1} for the same material at 800 °C [25]. One can estimate the thickness of chromia after 40,000 h using these two constants and a chromia density of 5.2 g cm^{-3} to be around 5–23 μm. On the other hand, actual scale thickness was found around 13–17 μm for Crofer22APU when oxidized in air for 8850 h at 800 °C [26]. Our sample pre-oxidized at 1200 °C/2 h appeared to be in this long-term oxidation range. The chemical composition of the oxide layer was found to be primarily Cr_2O_3, with a thin, discrete layer of $(Cr,Mn)_3O_4$ spinel on top of the Cr_2O_3 layer (arrow in Fig. 3A); this is consistent with previous studies [14,27]. The scale thickness of the sample pre-oxidized at 800 °C/2 h was lower (<0.5 μm), and should be negligible for the as-received (un-oxidized) steel, although the as-received samples could still form some oxide scale during the sealing process before the glass powders melted and sealed off the oxygen. The relatively thick Cr_2O_3 oxide layer on the 1200 °C/2 h oxidized sample did not spall off after cooling, suggesting good adhesion strength even though the Cr_2O_3 had a low CTE (~9×10^{-6}/°C) compared to the parent metal and was therefore expected to be under residual compressive stress. The 1200 °C/2 h oxidized sample also showed some undesirable pore formation underneath the thick oxide layer (Fig. 3B).

3.3. Room temperature seal strength of pre-oxidized samples

Overall, all the samples (as-received and pre-oxidized) showed good bonding without fracture after sealing at elevated temperature and cooling down to room temperature. Room temperature seal strengths of the joined metal/glass/metal couples are shown in Fig. 4. The strength of as-sealed samples was 6.3 ± 0.9 MPa, and was 6.3 ± 0.9 MPa for samples pre-oxidized at 800 °C/2 h. The strength of samples pre-oxidized at 1000 °C/2 or 1200 °C/2 h showed a distinct reduction to 2.6 ± 0.8 and 2.9 ± 0.4 MPa, respectively. This indicates that the seal strength was degraded if the thickness is greater than ~1–2 μm while scales thinner than ~0.5 μm had no effect on strength. It should be noted that the term "seal strength" is used due to the intended application of the material, although the more conventional terms "joint or interfacial strength" could be used for the specific properties measured in this study. The measured seal strengths were one to two orders of magnitude lower than the individual strength of the bulk glass or typical SOFC components. For example, NiO/YSZ porous anode supports were reported to have a bend strength ranging from 56 to 200 MPa depending on the porosity and test methods, and YSZ electrolyte was much stronger [28]. The strengths of ferritic stainless steels were also very high at room temperature (>300 MPa). The bend

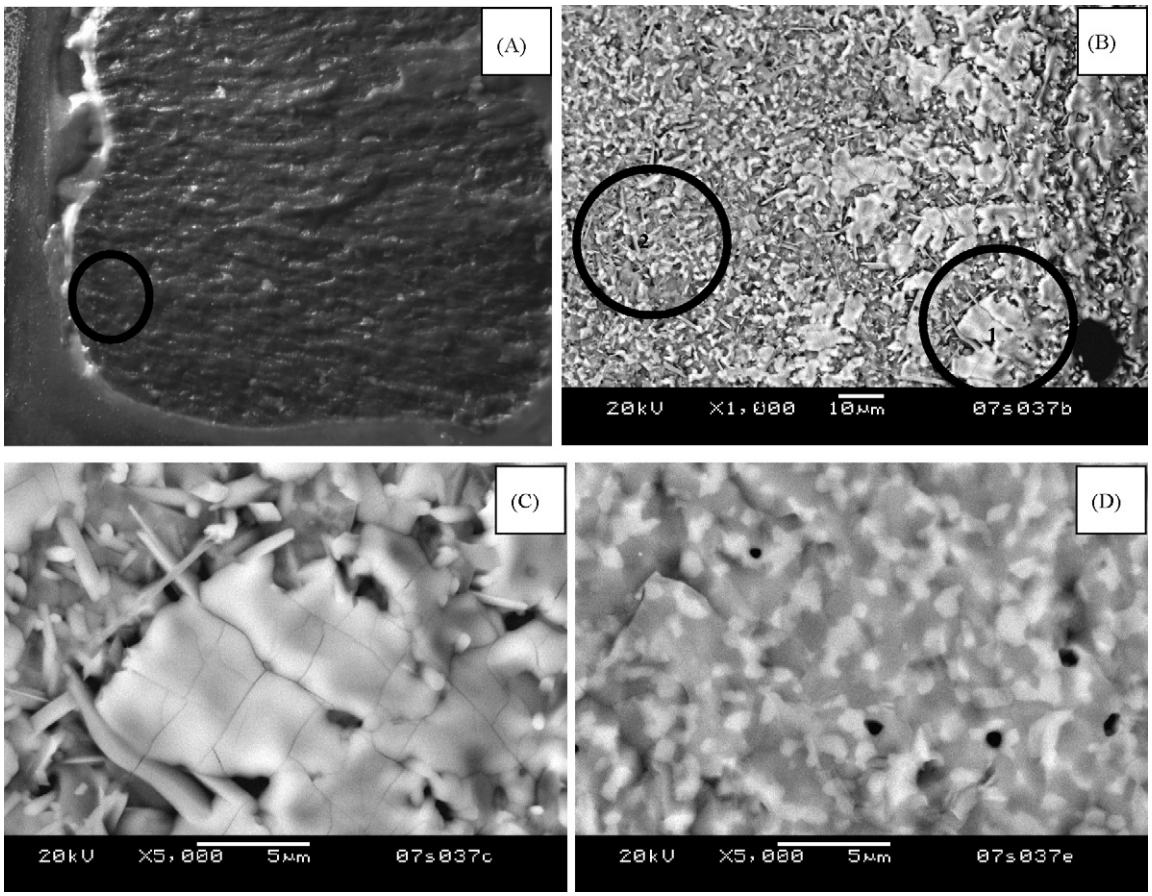

Fig. 7. Optical and SEM micrographs of the fracture surface of as-sealed as-received sample. (A) Optical micrograph shows that fracture initiated from the sealing edges; (B) SEM image of the circled area in (A); (C) and (D) high magnification images of circled areas in (B) showing regions with micro-cracked large grains, and regions with fine features.

strength of a typical SOFC sealing glass (e.g. Ba–Ca–Al–B–SivO) was 84 ± 14 MPa [29]. No joint or interfacial strengths for SOFC sealing glass bonded with metallic interconnect were found in the literature. The results of the present study indicate that the seals would likely be the weakest link in an assembled planar stack, where multiple tens of repeating unit cells may be joined with seals. The cause of the observed low strengths will be discussed in the next section. Fig. 5 shows the load and displacement curve for the seal strength test of an as-sealed coupon. Samples with pre-oxidized samples showed similar behavior. Clearly, the curve exhibited typical catastrophic brittle failure with load dropping at the maximum point, with no sign of nonlinearity, microcracking, or gradual damage during the test.

3.4. Effect of environment on seal strength of aged samples

As SOFC sealants are exposed to both oxidizing and reducing environments during operation, it is important to understand the effect of environment on seal strength, especially for planar SOFCs which are expected to last for tens of thousand of hours with repeated thermal cycling. Two additional sets of as-sealed samples were aged in different gases to assess the environmental effect on mechanical integrity of the seals. The seal strength of samples aged in air or a wet reducing environment are plotted in Fig. 6, together with the data of unaged samples from Fig. 4. It is evident that the strength degraded substantially after aging in air (850 °C/500 h), dropping to 0.5 ± 0.3 MPa. On the other hand, no strength degradation was observed for samples aged in the wet reducing environment (850 °C/250 h). The strength of those samples was 7.0 ± 1.6 MPa, which was slightly higher than that of the unaged samples (6.3 ± 0.9 Mpa). The severe strength degradation of samples aged in air appeared to be consistent with the strength data of the pre-oxidized samples discussed above, and was related to interfacial reaction in the oxidizing environment between SrO or $SrSiO_3$ (from the sealing glass) and Cr_2O_3 (from the metal scale) [6]:

$$2SrO(s) + Cr_2O_3(s) + 1.5O_2(g) \rightarrow 2SrCrO_4(s) \quad \Delta G_{800-900^\circ C} = -(135\text{–}145)\,\text{kJ mol}^{-1} \tag{1}$$

$$2SrSiO_3(s) + Cr_2O_3(s) + 1.5O_2(g) \rightarrow 2SrCrO_4(s) + 2SiO_2(s) \quad \Delta G_{800-900^\circ C} = -(4\text{–}14)\,\text{kJ mol}^{-1} \tag{2}$$

The negative Gibbs free energies indicates that strontium chromate can form spontaneously in air, and that chromate formation may be more favorable from "SrO" in an un-crystallized glassy phases rather than from the crystallized $SrSiO_3$. Both $SrCrO_4$ and $BaCrO_4$ have been observed at glass/metal interfaces exposed to air when the metal was a Cr-containing ferritic steel [6,14]. Chromate formation has not been observed in reducing environments, which is consistent with the positive Gibbs free energy calculated under those conditions [6]. For the case of $SrCrO_4$ the equilibrium oxygen partial pressure was calculated to be 2.5×10^{-8} atm (800 °C) and therefore would not form in the reducing environment where PO_2

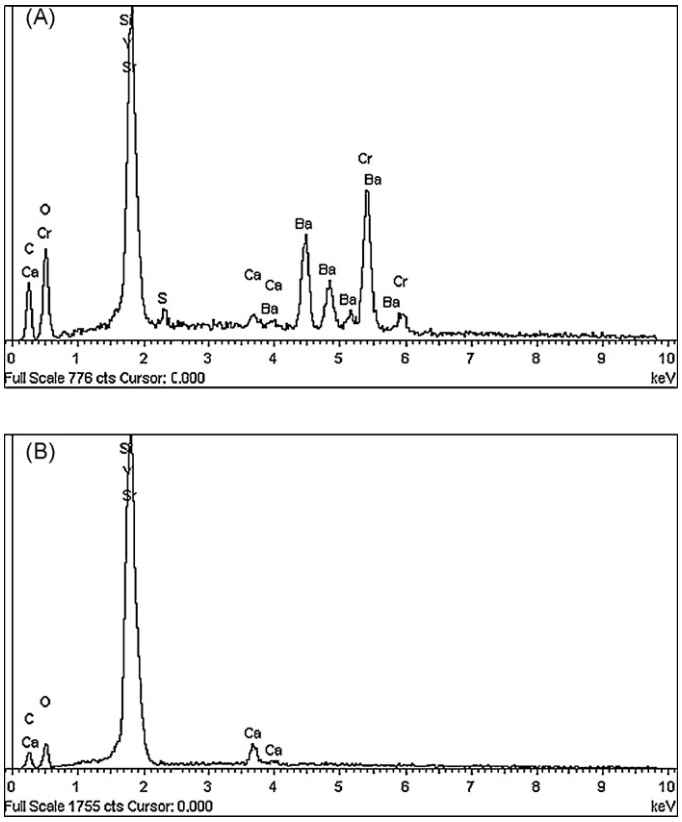

Fig. 8. EDS of the selected areas (point #1 and #2) from Fig. 7(B) showing (A) the region with micro-cracked large grains containing an appreciable amount of Cr, and (B) the region away from the sealing edge, which was free of Cr.

was less than 10^{-19} atm. Due to the very high CTE of these chromates ($22–23 \times 10^{-6}\,^{\circ}C^{-1}$), high residual tensile stresses would be expected to build up during cooling, leading to severe strength degradation. The reason for the slight strength increase for the samples aged in the reducing environment is not clear, but may be related to changes in flaw morphology/size or relaxation of residual stresses when samples were held at elevated temperatures.

3.5. Fracture surface and interfacial microstructure analysis

The fracture of as-sealed samples, whether the metal coupons were as-received or pre-oxidized, all showed similar fractography with most of the fractures originating from the outer boundary of sealing glass, where oxygen was available for interfacial reaction. Fig. 7A is a typical low magnification optical micrograph which reveals the hackle lines pointing toward the failure origin, i.e., along the sealing edges. Scanning electron microscopy (Fig. 7B) revealed regions of larger grains (Fig. 7C) and finer grains (Fig. 7D). It was noted that the larger grains were all micro-cracked (Fig. 7C). EDS point analysis (Fig. 8) of the two regions (points #1 and #2 in Fig. 7B) indicated that the micro-cracked large grains contained an appreciable amount of Cr, while the regions away from the edge with finer precipitates/crystallites showed the typical glass composition with no trace of Cr. It is interesting to note that Ba (a significant impurity in the $SrCO_3$ raw material) appeared to be concentrated at the edge regions as shown in Fig. 8B, suggesting Ba is more reactive with Cr than Sr. Similar Ba depletion was observed in a similar sealing glass (Ba–Ca–Al–B–Si–O) when joined with SS446 alloy [27]. The calculated Gibb's free energy of formation for $BaCrO_4$ (based on a reaction analogous to Eq. (1)) was found to be $-207\,kJ\,mol^{-1}$, which is more favorable than the value for $SrCrO_4$ of $-144\,kJ\,mol^{-1}$. In a cross-section view, the formation of an interfacial reaction zone near the outer sealing edges of the glass/metal interface was clearly evident, as shown in Fig. 9A (arrow), and much less evident at locations away from the sealing edges (Fig. 9B). Overall, the current fractography and chemical analyses strongly suggest that the large micro-cracked grains were $SrCrO_4$: (1) Pure $SrCrO_4$ is yellow and yellowish color was observed on the fracture surfaces along the circumference. (2) EDS analyses showed the presence of a substantial amount of Cr in these grains. (3) Microcracking in ceramics is often observed when the ceramic material experiences large volume changes from phase transformation during cooling, such as ZrO_2 (due to tetragonal to monoclinic phase transition) or $PbTiO_3$ (due to large CTE anisotropy). Pure $SrCrO_4$ is orthorhombic and highly anisotropic in CTE with $\alpha_a = 16.5 \times 10^{-6}\,K^{-1}$, $\alpha_b = 33.8 \times 10^{-6}\,K^{-1}$, and $\alpha_c = 20.4 \times 10^{-6}\,K^{-1}$ [30]. Also, the CTE of the glass matrix is only $11.8 \times 10^{-6}\,K^{-1}$, so the chromates grains would be under large tensile stresses during cooling and therefore likely to crack. (4) The formation of $SrCrO_4$ is thermodynamically favorable only if oxygen is available, as it is in the circumferential region. Therefore the strength degradation for samples pre-oxidized at 1000 and 1200 °C/2 h as well as samples aged in air 850 °C/500 h could be attributed to continuous chromate formation along the glass/metal interfaces over time resulting in larger critical flaws and therefore lower strength. The observed strength degradation of silicate sealing glasses containing alkaline earths, particularly Ba and Sr, clearly indicates the potential failure of SOFC stack seals if bare Cr-containing alloys are used as metallic interconnect materials. Remedies for this undesirable interfacial reaction such as alu-

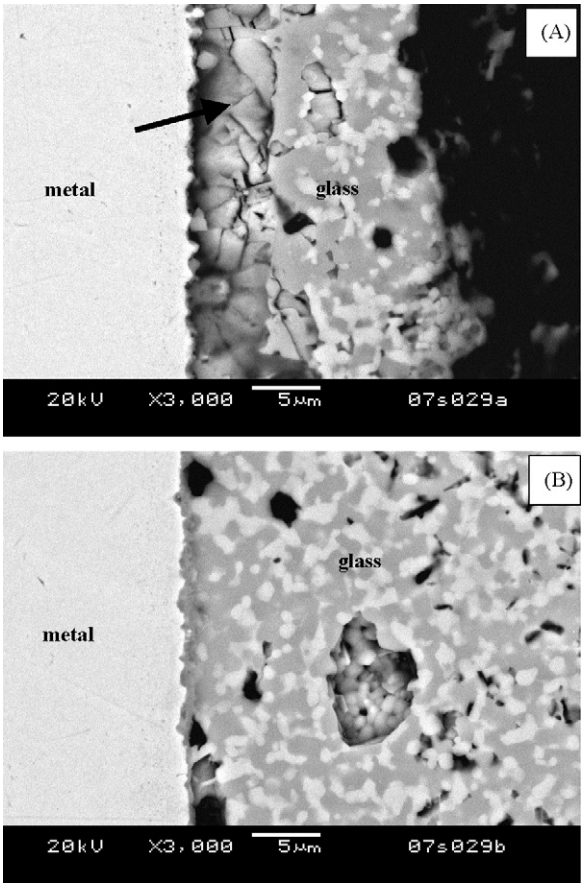

Fig. 9. Cross-section view of the glass/metal (as-received) interface: (A) region close to seal outer edge showing distinct interfacial reaction zone (arrow), and (B) region away from the sealing edge.

minization of the metal surface are under investigation and will be reported in the near future.

4. Summary and conclusion

A novel alkaline-earth aluminosilicate sealing glass was developed with stable thermal properties. The glass was sandwiched between two metal coupons to evaluate the mechanical strength. Joins with pre-oxidized metal coupons showed a large strength degradation for samples heat-treated above 1000 °C. Strength was drastically reduced when for joins aged in air for 500 h. Fracture surface analysis, spot chemical analysis, and thermodynamic calculations revealed the formation of $SrCrO_4$ and/or $BaCrO_4$ along the edges of the glass/metal interfaces. This chromate formation is believed to be the cause of the observed strength degradation due to high CTE and anisotropy. It is concluded that a protective coating will likely be needed if Cr-containing ferritic stainless steels are to be used as metallic interconnect materials for SOFCs.

Acknowledgements

The authors would like to thank S. Carlson for SEM sample preparation, and J. Coleman for SEM analysis. This work summarized in this paper was funded by the US Department of Energy's Solid-State Energy Conversion Alliance (SECA) Core Technology Program. The authors would like to thank Wayne Surdoval, Mani Manivannan, and Briggs White from NETL for helpful discussions. Pacific Northwest National Laboratory is operated by Battelle Memorial Institute for the US Department of Energy under Contract no. DE-AC06-76RLO 1830.

References

[1] N.Q. Minh, J. Am. Ceram. Soc. 76 (3) (1993) 563–588.
[2] B.C.H. Steele, J. Mater. Sci. 36 (2001) 1053–1068.
[3] S.C. Singhal, in: S.C. Singhal, M. Dokiya (Eds.), Solid Oxide Fuel Cells (SOFC VI) Proceedings of the Sixth International Symposium, vol. 99–19, The Electrochemical Society, 1999, pp. 39–51.
[4] R. Bolden, K. Foger, T. Pham, in: S.C. Singhal, M. Dokiya (Eds.), Solid Oxide Fuel Cells (SOFC VI) Proceedings of the Sixth International Symposium, vol. 99–19, The Electrochemical Society, 1999, pp. 80–87.
[5] A. Khandkar, S. Elangovan, J. Hartvigsen, D. Rowley, R. Privette, M. Tharp, in: S.C. Singhal, M. Dokiya (Eds.), Solid Oxide Fuel Cells (SOFC VI) Proceedings of the Sixth International Symposium, vol. 99–19, The Electrochemical Society, 1999, pp. 88–94.
[6] Y.-S. Chou, J.W. Stevenson, P. Singh, J. Electrochem. Soc. 154 (7) (2007) B644–B651.
[7] N. Lahl, K. Singh, L. Singheiser, K. Hilpert, D. Bahadur, J. Mater. Sci. 35 (2000) 3089–3096.
[8] S.-B. Sohn, S.-Y. Choi, G.-H. Kim, H.-S. Song, G.-D. Kim, J. Non-crystalline Solids 297 (2002) 103–112.
[9] K.L. Ley, M. Krumpelt, R. Kumar, J.h. Meiser, I. Bloom, J. Mater. Res. 11 (6) (1996) 1489–1493.
[10] S. Taniguchi, M. Kadowaki, T. Yasuo, Y. Akiyama, Y. Miyake, K. Nishio, J. Power Sources 90 (2) (2000) 163–169.
[11] X. Qi, F.T. Akin, Y.S. Lin, J. Membr. Sci. 193 (2001) 185–193.
[12] V.A.C. Haanappel, V. Shemet, S.M. Gross, Th. Koppitz, N.H. Menzler, M. Zahid, W.J. Quadakkers, J. Power Sources 150 (2) (2005) 86–100.
[13] N. Lahl, D. Bahadur, K. Singh, L. Singheiser, K. Hilpert, J. Electrochem. Soc. 149 (5) (2002) A607–614.
[14] Z. Yang, K.D. Meinhardt, J.W. Stevenson, J. Electrochem. Soc. 150 (8) (2003) A1095–A1101.
[15] K.S. Weil, J.S. Hardy, J.Y. Kim, J. Adv. Specialty Mater. V Am. Soc. Met. 5 (2000) 47–55.
[16] J. Duquette, A. Petric, J. Power Sources 137 (1) (2004) 71–75.
[17] M.C. Tucker, C.P. Jacobson, L.C. De Jonghe, S.J. Visco, J. Power Sources 160 (2) (2006) 1049–1057.
[18] K.S. Weil, C.A. Coyle, J.T. Darsell, G.G. Xia, J.S. Hardy, J. Power Sources 152 (1) (2005) 97–104.
[19] S.P. Simner, J.W. Stevenson, J. Power Sources 102 (1–2) (2001) 310–316.
[20] Y.-S. Chou, J.W. Stevenson, J. Power Sources 112 (1) (2002) 130–136.
[21] Y.-S. Chou, J.W. Stevenson, J. of Power Sources 125 (1) (2004) 72–78.
[22] P. Lessing, J. Mater. Sci. 42 (2007) 3465–3476.
[23] J.W. Fergus, J. Power Sources 147 (1) (2005) 46–57.
[24] S. Fontana, R. Amendola, S. Chevalier, P. Piccardo, G. Caboche, M. Viviani, R. Molins, M. Sennour, J. Power Sources 171 (2) (2007) 652–662.
[25] P. Huczkowski, N. Christianson, V. Shemet, J. Piron-Abellan, L. Singheiser, W.J. Quadakkers, Mater. Oxid. 55 (11) (2004) 825–830.
[26] Z. Yang, J.W. Stevenson, unpublished data.
[27] Z. Yang, K. Scott, D.M. Paxton, J.W. Stevenson, J. Electrochem. Soc. 159 (9) (2003) A1188–A1201.
[28] N.M. Sammes, Y. Du, J. Mater. Sci. 38 (2003) 4811–4816.
[29] Y.S. Chou, unpublished data.
[30] C.W.F.T. Pistorius, M.C. Pistorius, Z. Kristallogr. 117 (1962) 259.